Supporting Information

Large-scale synthesis of zinc oxide-supported indium single-atom for efficient electrocatalytic CO_2 reduction reaction

Wenzhao Duan[a,5], Tianrui Lu[a,5], Qiuyue Xiang [a,5], Heng Chen[c,*], Xi Yu [a], Ge Meng[a], Zheng-Jun Wang[a,*], Hailong Zhang [d], Lilong Zhang[e,*], Huile Jin[a], Shun Wang[a], Jing-Jing Lv[a,b,*]

[a]College of Chemistry and Materials Engineering, Wenzhou University, Wenzhou, Zhejiang 325035, China

[b]State Key Laboratory of Clean Energy Utilization, College of Energy Engineering, Zhejiang University, Hangzhou 310027, P. R. China

[c] State Key Laboratory of Heavy Oil Processing, China University of Petroleum (Beijing), Beijing 102249, China

[d] State Key Laboratory for Advanced Metals and Materials, University of Science and Technology Beijing, Beijing 100083, China.

[e]State Key Laboratory of Materials-Oriented Chemical Engineering, College of Chemical Engineering, Nanjing Tech University, Nanjing, 211816, China

[5]These authors contributed equally: Wenzhao Duan, Tianrui Lu, and Qiuyue Xiang

Email: 2025310353@student.cup.edu.cn; zhengjunwang@wzu.edu.cn; zhanglilong@njtech.edu.cn; jjlyu@wzu.edu.cn

Experimental Section

Synthesis of ZnO@In-SACs

At room temperature, ZnO@In-SACs were synthesized via a rapid coprecipitation in a Micro Impinging Stream Reactor (MISR). Specifically, zinc nitrate hexahydrate ($Zn(NO_3)_2·6H_2O$) and indium nitrate hexahydrate ($In(NO_3)_3·6H_2O$) were dissolved in deionized water with vigorous stirring to prepare a Zn^{2+}-In^{3+} mixed solution with a total concentration of 0.48 mol L^{-1} (Zn^{2+}/In^{3+} molar ratio = 10:1). Meanwhile, a 0.855 mol L^{-1} sodium hydroxide (NaOH) precipitant solution was prepared. The two solutions

were simultaneously pumped into MISR using high-flow-rate peristaltic pumps. The high-speed impingement of the two streams enabled rapid mixing and the precipitation reaction. The resulting suspension was aged at room temperature for 12 hours, followed by centrifugal separation. The solid precipitate was sequentially washed three times with deionized water and ethanol. The final product was dried at 60 °C and ground into a powder, yielding approximately 692 grams per batch. For comparison, pure ZnO and In $(OH)_3$ were also synthesized in the MISR using the same method as described for ZnO@In-SACs by individually introducing $Zn(NO_3)_2 \cdot 6H_2O$, and $In(NO_3)_3 \cdot 6H_2O$. The lab-scale batch was prepared (1.54 g, denoted as ZnO@In-SACs-L) following the identical procedure as ZnO@In-SACs by decreasing the dosage of $Zn(NO_3)_2 \cdot 6H_2O$) and $In(NO_3)_3 \cdot 6H_2O$.

Synthesis of ZnO-20@In-SACs and ZnO-100@In-SACs

ZnO-20@In-SACs and ZnO-100@In-SACs were synthesized using a procedure identical to that of ZnO@In-SACs, except that the molar ratios of Zn^{2+}/In^{3+} in the initial precursor solutions were adjusted to 20:1 and 100:1, respectively.

Synthesis of ZnO@In-SACs-300 °C

The ZnO@In-SACs-300 °C sample was prepared by calcining the as-synthesized ZnO@In-SACs powder in a tube furnace at 300 °C for 3 hours under a flowing H_2/Ar (5 vol% H_2) atmosphere, with a heating rate of 5 °C min^{-1}.

Materials characterization

The morphology and microstructure were characterized by Scanning electron microscopic (SEM) using a Nova 200 NanoSEM operated at an acceleration voltage of 20 kV. The transmission electron microscopy (TEM), and high-resolution TEM (HRTEM) using a JEM-2100F TEM operating at 200 kV. The SEM images were taken directly by coating the sample on a gas diffusion layer (GDL, Fuel Cell Store). The TEM sample was acquired by scraping off from the sample coated GDL. The XRD measurements were conducted on a D8 ADVANCE X-ray diffractometer (Bruker Corporation, America). A Thermo Scientific K-Alpha XPS System was used and XPS fitting was conducted by Avantage software with the adventitious carbon peak being

calibrated to 284.8 eV. The metal loading was quantified by inductively coupled plasma optical emission spectrometry (ICP-OES) using a PerkinElmer Optima 8000 spectrometer.

Preparation of catalyst ink and electrode

To prepare the catalyst ink, 25 mg of catalyst was ultrasonically dispersed in the mixture of 3 mL of *n*-propanol, 500 μL of multiwalled carbon nanotubes (MWCNTs, 95%, XFNANO) solution (10 mg MWCNTs dispersed in 10 mL tetrahydrofuran (THF)) and 20 μL of Nafion (10 wt% aqueous solution, Fuel Cell Store, America). The mixture was sonicated for 30 min for the dropcasting. The MWCNTs were used to facilitate conductivity.[1] The carbon paper with a microporous layer (Sigracet 29 BC, Fuel Cell Store) was used as the GDL for supporting catalyst and collecting current. At a loading of 0.5 mg cm^{-2}, the catalyst was coated on 1×2 cm^2 GDL as the working electrode. The nickel foam was used as the counter electrode and Ag/AgCl (saturated KCl) as the reference electrode.

Electrochemical measurements

Electrochemical measurements were conducted on an electrochemical workstation (Autolab M204) in a three-electrode system. CO_2 electroreduction was measured in a three-channel flow cell with compartments measuring 2 * 0.5 * 0.15 cm^3. The electrode area was 1 cm^2, and the distance between the electrode and the membrane was 2 mm. An external Ag/AgCl reference electrode, located approximately 5 cm from the cathode, was used to measure the cathodic half-cell potential. All potential measurements were converted to the RHE scale using the formula: $E_{RHE} = E_{Ag/AgCl} + E^{\theta}_{Ag/AgCl} + 0.059 \times pH$ (in volts). The pH values of the bulk electrolyte after electrolysis were used for RHE conversions unless otherwise stated. The device was fabricated from acrylic plastic and contained a gas compartment for flowing CO_2, anode and cathode channels for flowing electrolyte, a membrane for separating the anode and cathode, and solid end pieces. Poly(tetrafluoroethylene) (PTFE) gaskets were placed between each component for sealing, and the device was tightened using six bolts.

The gas flow rate into the flow cell was set as 15 sccm via a mass flow controller (Alicat Scientific). The catholyte flow rates were controlled via a peristaltic pump (YZ1515x, Baoding Chuangrui Precision Pump CO., LTD), with the catholyte flow rate ranging from 0.1 to 1 mL min^{-1} depending on the current densities (lower flow rates were used at lower current densities to allow for sufficient accumulation of liquid products). The anolyte flow rate was 2 mL min^{-1}. An anion exchange membrane (FAA-3, Fumatech) was used in 1 M KOH. The backpressure of the gas in the flow cell was tuned to atmospheric pressure as controlled by a backpressure controller (Alicat Scientific). Each reported data point reflected the mean of at least three measurements, where the error bars were the standard deviation.

Gas products were quantified on a Multigas #5 gas chromatography (GC, SRI Instruments) equipped with a HayeSep D and Molsieve 5A columns connected to a thermal conductivity detector (TCD) and a HayeSep D column connected to a flame ionization detector (FID).

Liquid products were quantified using a Bruker AVIII 500 MHz NMR spectrometer. Typically, 500 μL of collected catholyte exiting the reactor was mixed with 100 μL D_2O containing 50 ppm (m/m) dimethyl sulphoxide (≥ 99.9%; Alfa) as the internal standard. The one-dimensional ^1H spectrum was measured with water suppression using a pre-saturation method.

Calculation of the specific current density per electrochemically active surface area

The electrochemically active surface area (ECSA) for all electrocatalysts was estimated from the electrochemical double-layer capacitance (C_{dl}). The C_{dl} value was determined based on the proportional relationship between the capacitive current and the scan rate, as defined by [2]:

$$C_{dl} = i_c / v$$

The cyclic voltammetry (CV) curves of the samples were measured in 0.1 M $HClO_4$ solution using a three-electrode configuration with an Ag/AgCl reference

electrode, at scan rates of 10, 20, 40, 60, 80, and 100 mV s^{-1}. The capacitive current (ic) at a specific potential was calculated using the equation $i_c = (j_a - j_c) / 2$, where j_a and j_c are the anodic and cathodic current densities, respectively. This calculated i_c value was then plotted against the scan rate (v), and the C_{dl} was obtained from the slope of the resulting linear plot.

Comment [ZW]: 引用文献

Faradaic efficiency (FE) measurements

Based on the definition of Faradaic efficiency[3]: $FE = Q_{Product} / Q_{total} = (Z \times n \times F)/Q_{total}$, where Z is the number of electrons transferred, n the number of moles for a given product, F Faraday's constant (96 485 C mol^{-1}), Q total all the charge passed throughout the electrolysis process (measured by calculating the curve area of current density *vs*. time plot).

Figures and Table

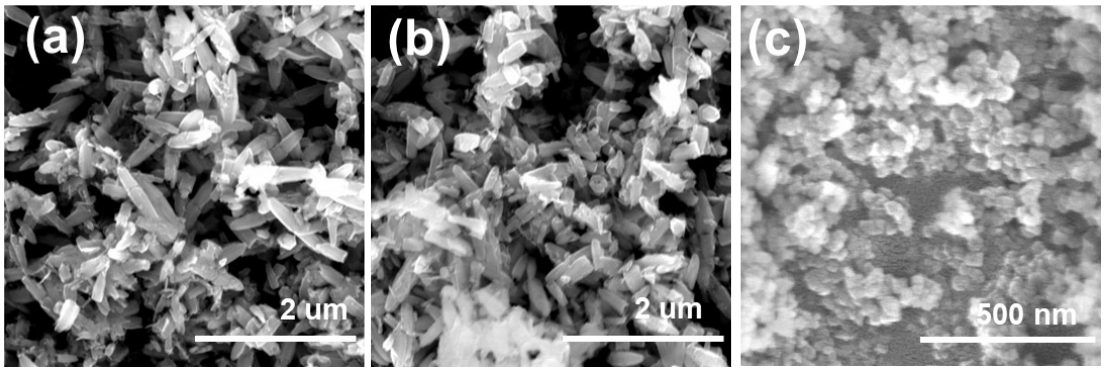

Fig. S1 SEM images of the (a) ZnO@In-SACs; (b) ZnO; and (c) In $(OH)_3$ before pre-reduction.

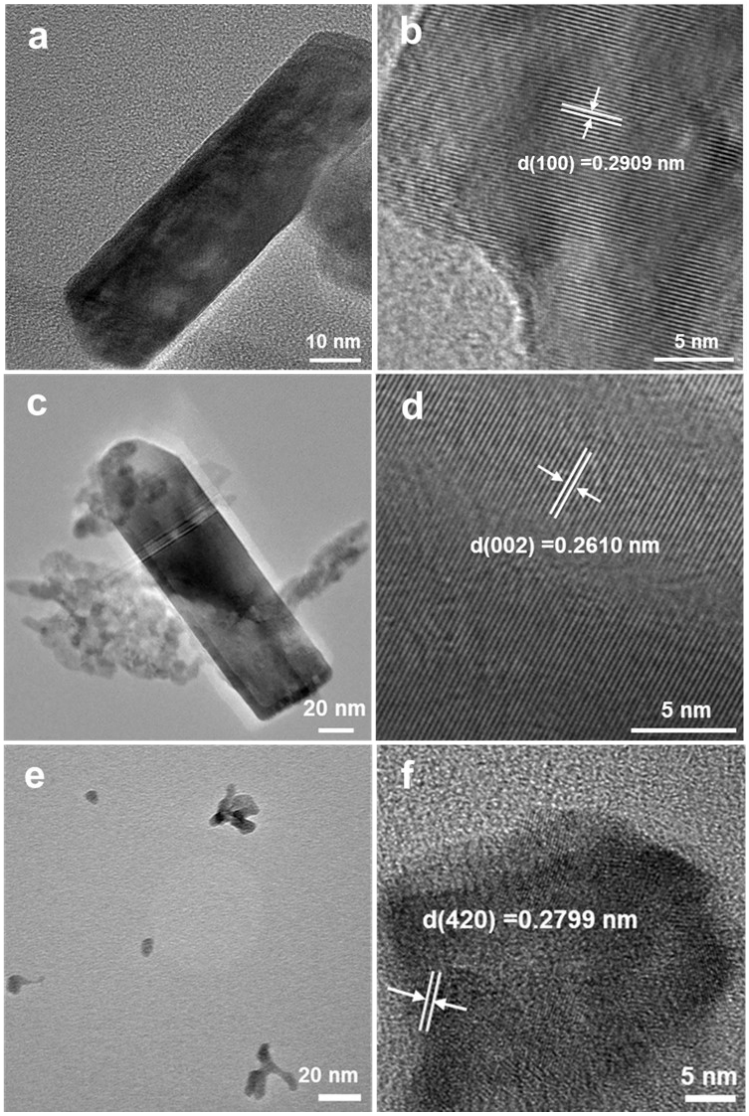

Fig. S2 The TEM and HRTEM images of (a-b) ZnO@In-SACs; (c-d) ZnO; and (e-f) $In(OH)_3$ before pre-reduction.

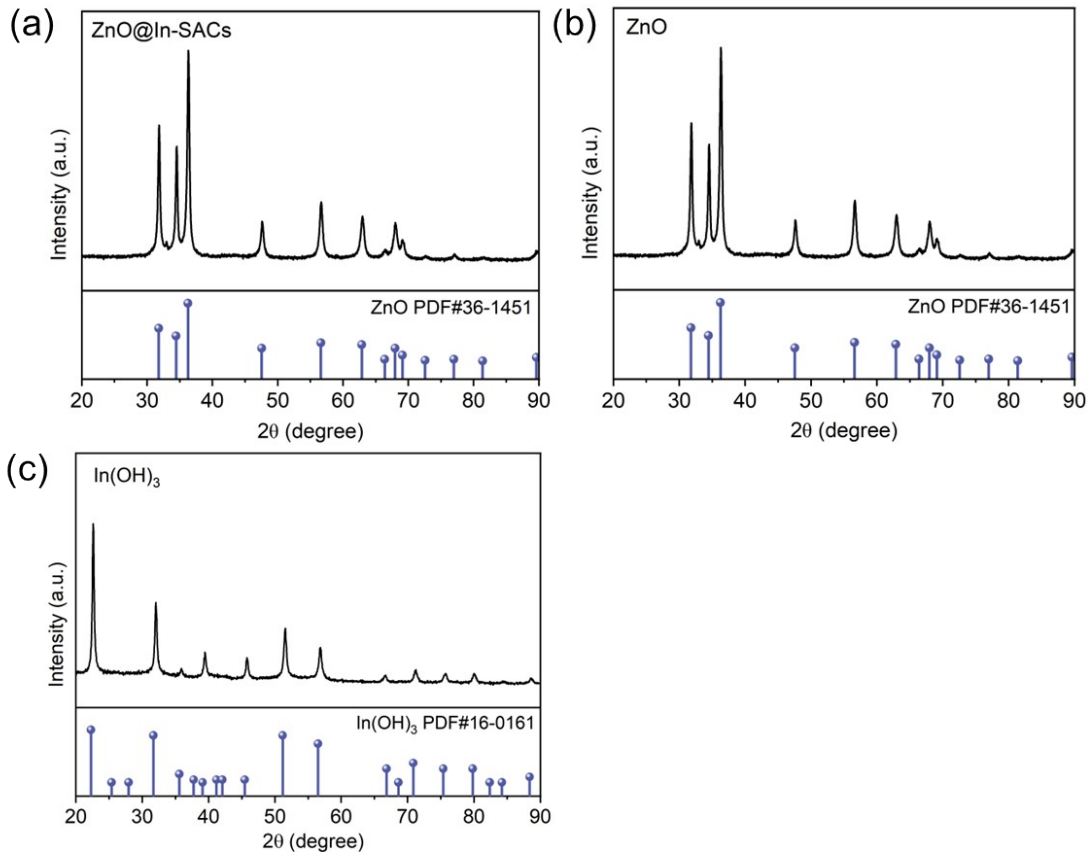

Fig. S3 XRD patterns of: (a) ZnO@In-SACs, (b) ZnO, and (c) $In(OH)_3$ before pre-reduction.

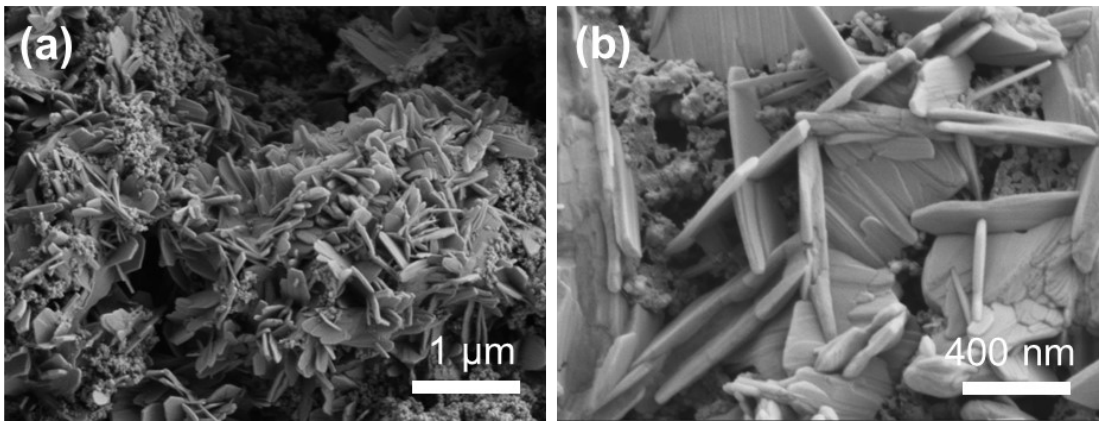

Fig. S4 (a-b) Representative SEM images of ZnO@In-SACs catalysts after 20 minutes pre-reduction.

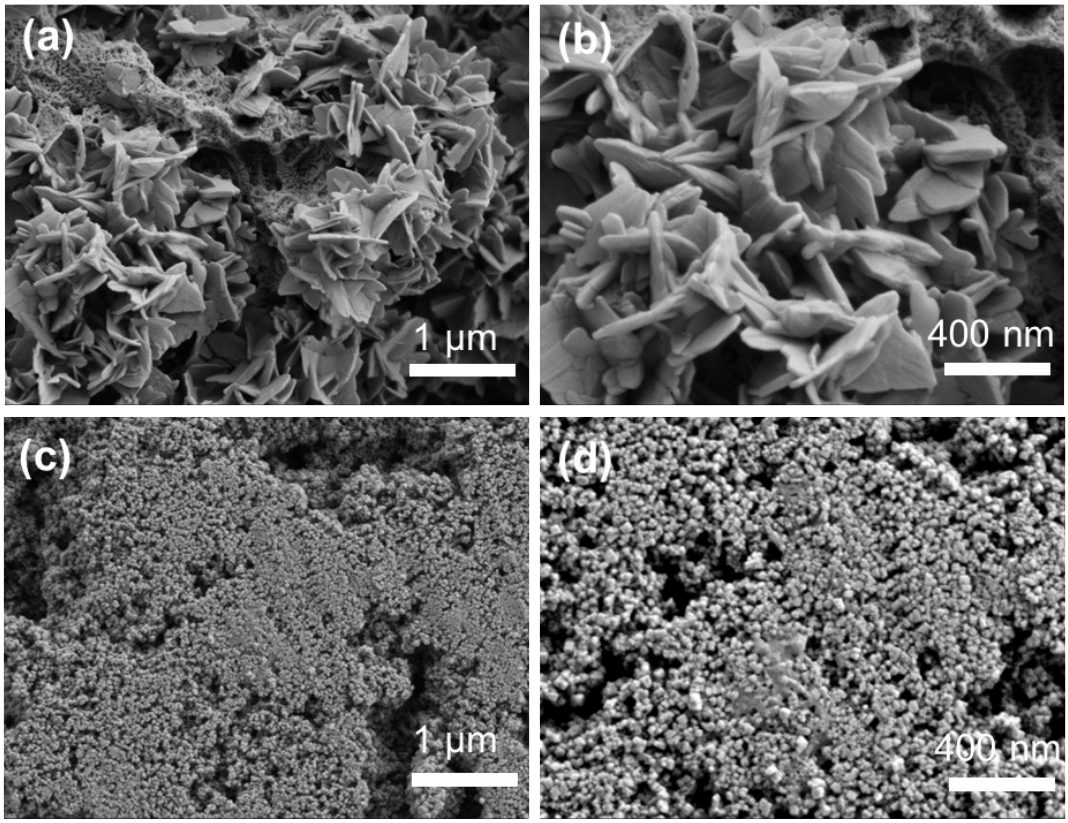

Fig. S5 Representative SEM images of (a-b) ZnO and (c-d) $In(OH)_3$ catalysts after 20 minutes pre-reduction.

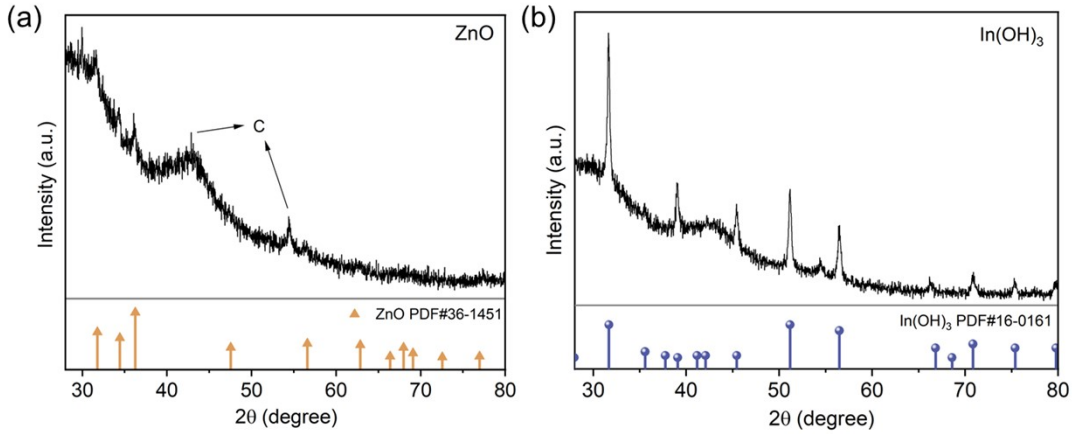

Fig. S6 XRD patterns of (a) ZnO, and (b) $In(OH)_3$ after 20 minutes pre-reduction.

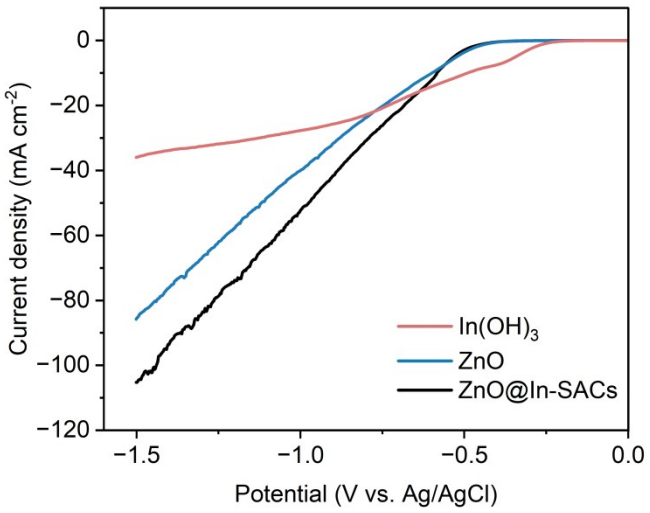

Fig. S7 LSV curves of ZnO@In-SACs, ZnO and $In(OH)_3$ after 20 minutes pre-reduction in 1.0 M KOH electrolyte.

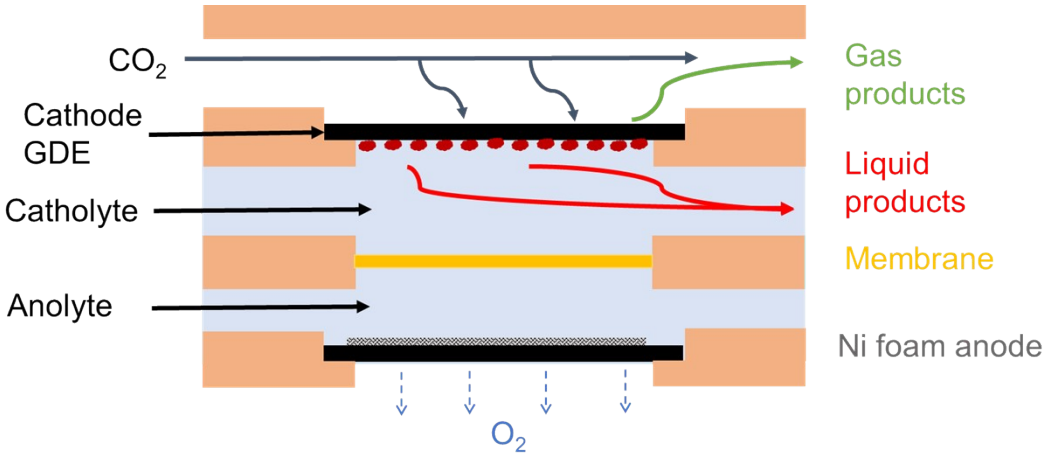

Fig. S8 Schematic diagram of the flow cell for eCO_2RR.

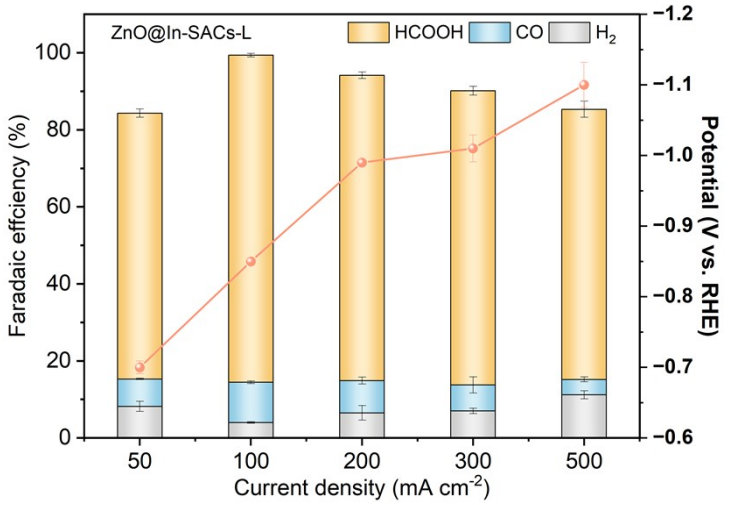

Fig. S9 eCO_2RR product distribution of (a) ZnO@In-SACs-L.

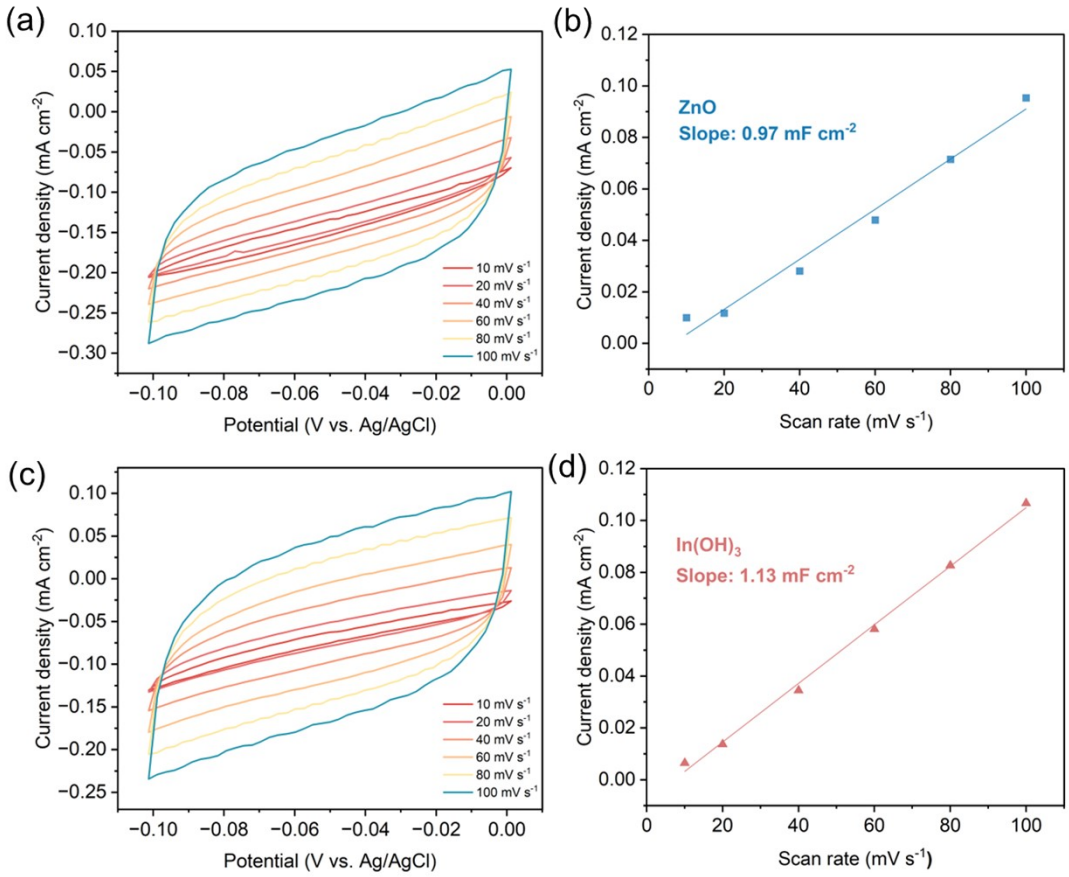

Fig. S10 (a) CV test for measuring double-layer capacitance (C_{dl}) of ZnO within the scan rate range of 10-100 mV·sec^{-1} and (b) C_{dl} of the electrode. (c) CV test for measuring double-layer capacitance (C_{dl}) of $In(OH)_3$ within the scan rate range of 10-100 mV·sec^{-1} and (d) C_{dl} of the electrode.

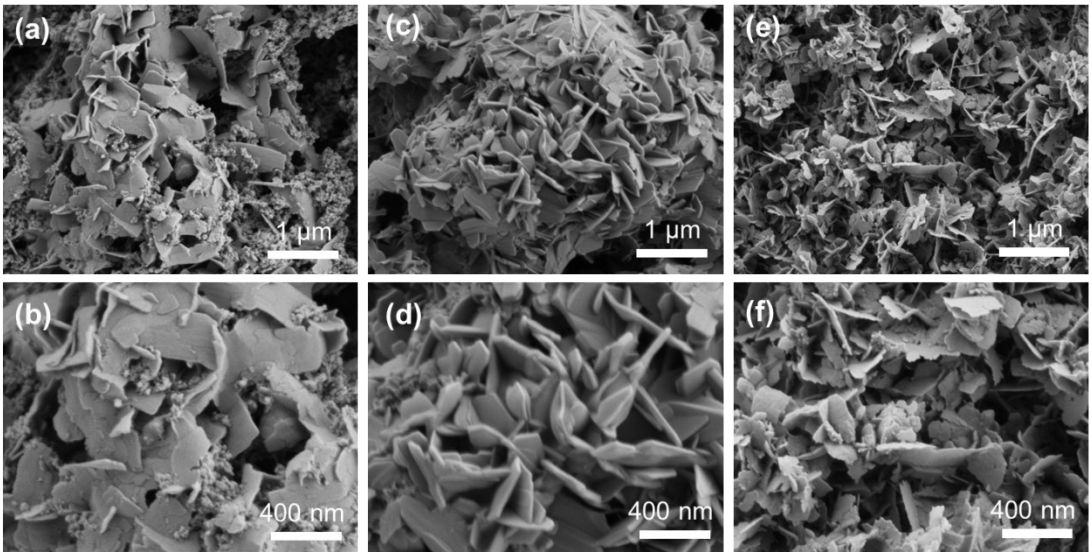

Fig. S11 Representative SEM images of (a-b) ZnO-20@In-SACs, (c-d) ZnO-100@In-SACs, and (e-f) ZnO@In-SACs-300 ℃ catalysts after 20 minutes pre-reduction.

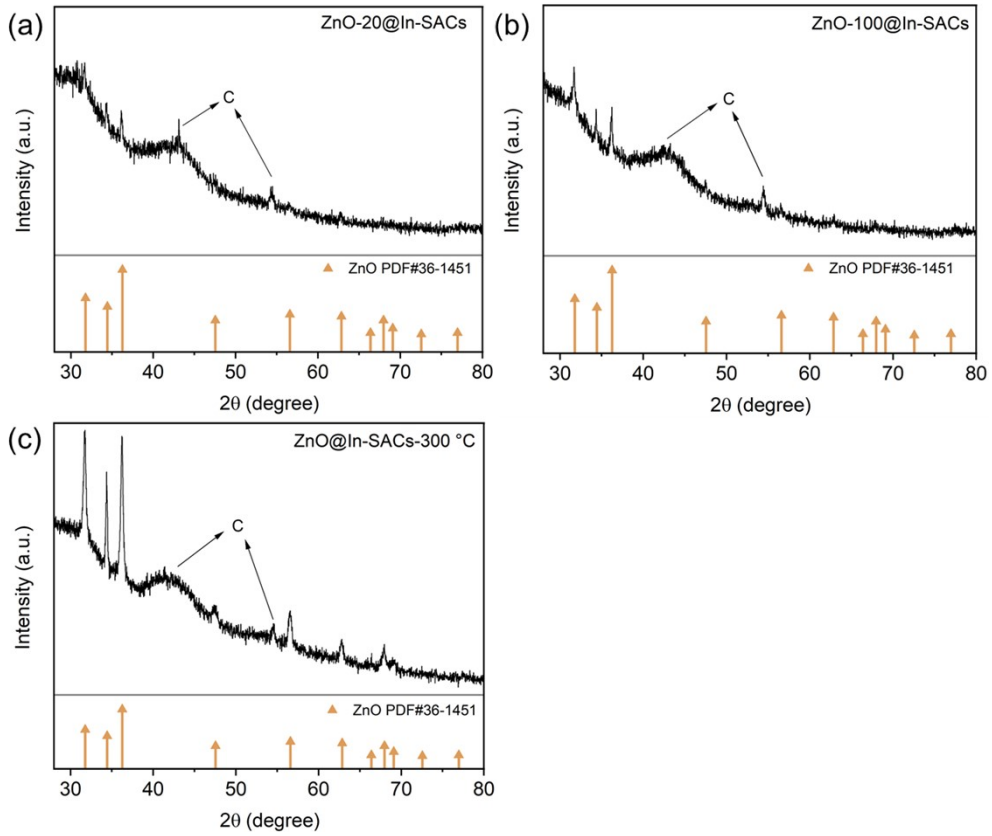

Fig. S12 XRD patterns of (a) ZnO-20@In-SACs , (b) ZnO-100@In-SACs, and (c) ZnO-@In-SACs-300 ℃ after 20 minutes pre-reduction.

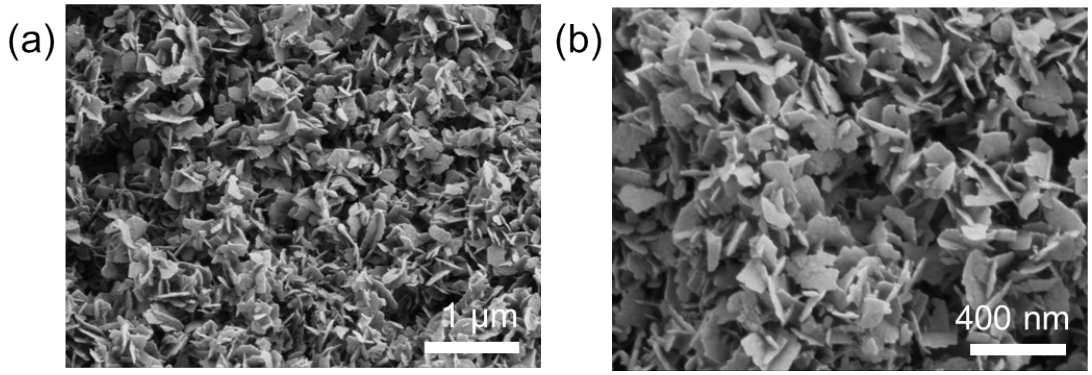

Fig. S13 SEM images of ZnO-@In-SACs after stability test.

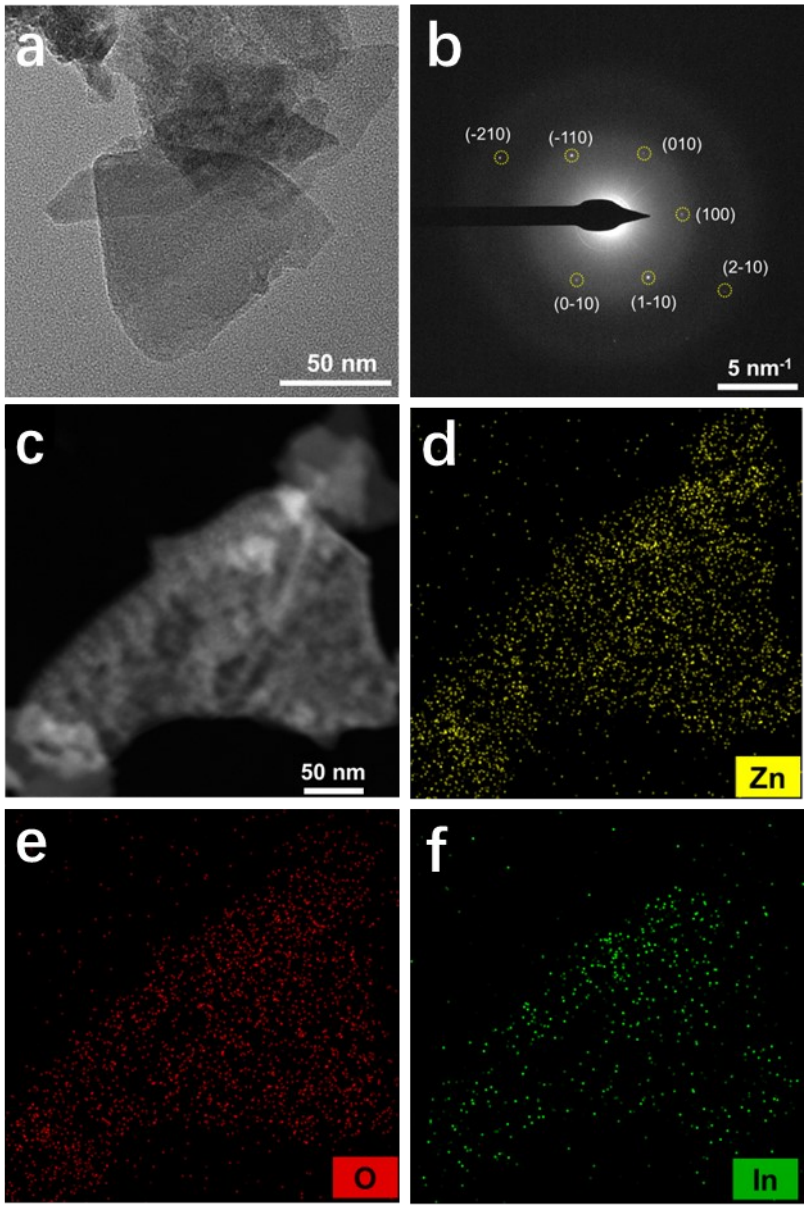

Fig. S14 (a) TEM image, (b) single-crystal diffraction pattern of the ZnO substrate indexed along the [00-1] zone axis, and (c-f) EDX elemental mapping analysis of ZnO-@In-SACs after stability test.

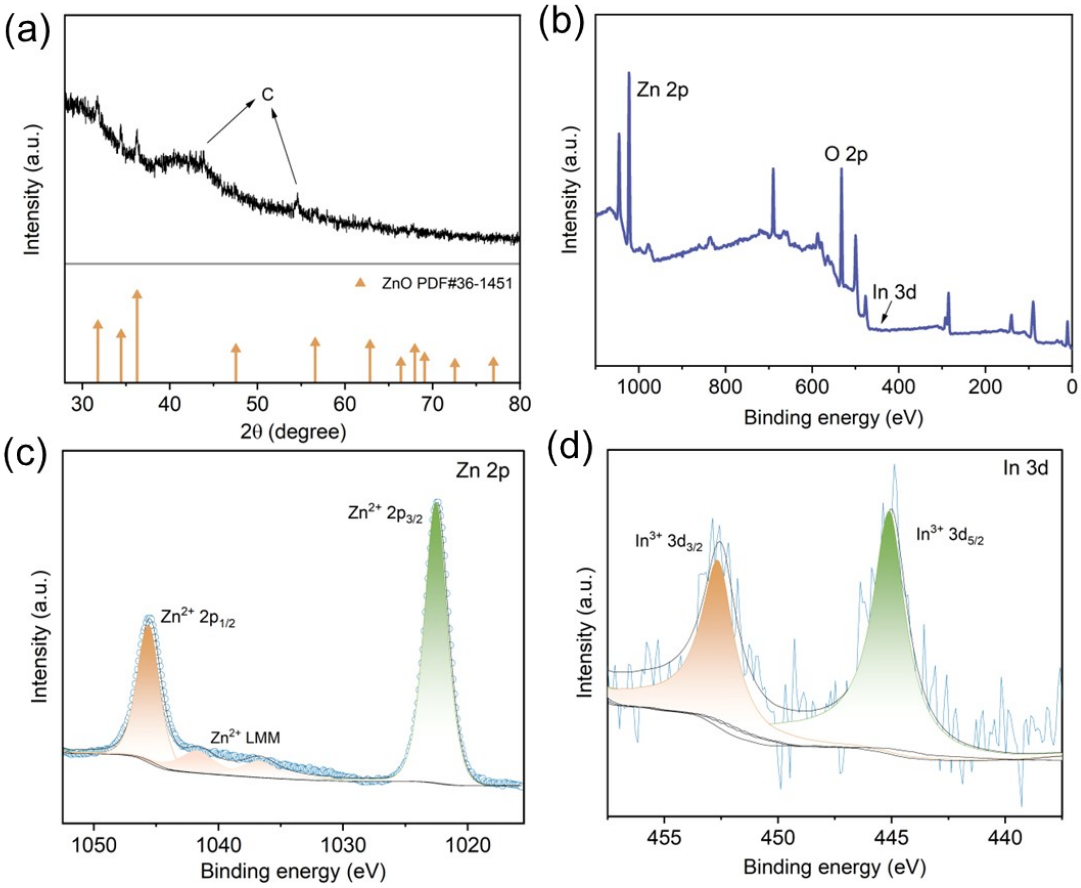

Fig. S15 (a) XRD pattern, (b) survey XPS spectrum, (c) Zn 2p and (d) In 3d XPS spectra of ZnO-@In-SACs after stability test.

Table S1 Catalytic performance comparison of various reported eCO_2RR catalysts with ZnO@In-SACs.

Catalysts	Electrolyte	Potential (V vs. RHE)	Current density (mA cm^{-2})	FE_{HCOOH} (%)	Stability (h)	Ref.
3.8%Cu-SnO_2	KOH	-0.9	-120	92	14	[4]
In_2O_3@C	KOH	-1.3	~ -155	94	9	[5]
In-O-ultrathin-SnS_2	$KHCO_3$	-1.2	22.7	88.6	15	[6]
$Bi_2O_2CO_3$-PABA	KOH	-1.1	-120	80	5	[7]
Bi@C-700-4	KOH	-0.8	~ -100	94.8	12	[3]
In@CNR	$KHCO_3$	-0.92	-50	88.4	12	[8]
CPs@In-MOFs	$KHCO_3$	-0.84	6.87	90.1	20	[9]
Cu_2S NSs	KOH	-1.2	-250	82	5	[10]
ZnO-@In-SACs	**KOH**	**-0.9**	**-100**	**85**	**40**	**This work**

Table S2 Comparison of the catalytic performance and batch yield between ZnO@In-SACs with other reported eCO_2RR catalysts produced via scalable methods for formate generation.

Catalysts	Batch yield (g)	Potential (V vs. RHE)	Current density (mA cm^{-2})	FE_{HCOOH} (%)	Stability (h)	Ref.
R-$BiCO_{2-x}$/ Bi_2O_3	1-10	-0.9	~ -35	92	65	[11]
$Bi_2O_2CO_3$	124.1	-1.4	~ -20	90	/	[12]
aMIL-68(In)-NH_2	16	-1.0	-129.9	92.9	22	[13]
ZnO-@In-SACs	**692.4**	**-0.9**	**-100**	**85**	**40**	**This work**

References

1. L. Zhou, C. Li, J.-J. Lv, W. Wang, S. Zhu, J. Li, Y. Yuan, Z.-J. Wang, Q. Zhang, H. Jin and S. Wang, *Carbon Energy*, 2023, **5**, e328.
2. Y. Yoon, B. Yan and Y. Surendranath, *J. Am. Chem. Soc.*, 2018, **140**, 2397-2400.
3. W. Guo, X. Cao, D. Tan, B. Wulan, J. Ma and J. Zhang, *Angew. Chem. Int. Ed.*, 2024, **63**, e202401333.
4. B. Li, J. Chen, L. Wang, D. Xia, S. Mao, L. Xi, S. Ying, H. Zhang and Y. Wang, *Appl. Catal. B Environ. Energy*, 2025, **363**, 124784.
5. Z. Wang, Y. Zhou, D. Liu, R. Qi, C. Xia, M. Li, B. You and B. Y. Xia, *Angew. Chem. Int. Ed.*, 2022, **61**, e202200552.
6. X. Zhang, M. Jiao, Z. Chen, X. Ma, Z. Wang, N. Wang, X. Zhang and L. Liu, *Chem. Eng. J.*, 2022, **429**, 132145.
7. L. Cao, J. Huang, X. Wu, Q. Xu, K. Su, Y. Zhong, M. Sun and L. Yu, *Appl. Catal. B Environ. Energy*, 2024, **358**, 124451.
8. B. Pan, G. Yuan, X. Zhao, N. Han, Y. Huang, K. Feng, C. Cheng, J. Zhong, L. Zhang, Y. Wang and Y. Li, *Small Science*, 2021, **1**, 2100029.
9. Z.-H. Zhu, B.-H. Zhao, S.-L. Hou, X.-L. Jiang, Z.-L. Liang, B. Zhang and B. Zhao, *Angew. Chem. Int. Ed.*, 2021, **60**, 23394-23402.
10. W. Liu, Y. Wen, N. Fang, M. Wang, Y. Xu and X. Huang, *Chem. Commun.*, 2023, **59**, 11843-11846.
11. X. Rong, Y. Zhao, C. Gao, L. Luo, X.-L. Lu and P. Chen, *J. Colloid Interface Sci.*, 2026, **703**, 139122.
12. M. Guo, G. Cao, X. He, G. Yang, H. Wang, Q. Zhang, Z. Liu and F. Peng, *J. Mater. Chem. A*, 2025, **13**, 37942-37952.
13. Z. Liu, X. Han, J. Liu, S. Chen, S. Deng and J. Wang, *ACS Appl. Mater.Inter.*, 2024, **16**, 28655-28663.